Spatiotemporal control of phosphatidylinositol 4-phosphate by Sac2 regulates endocytic recycling

FoSheng Hsu, Fenghua Hu, and Yuxin Mao

Weill Institute for Cell and Molecular Biology and Department of Molecular Biology and Genetics, Cornell University, Ithaca, NY 14853

It is well established that the spatial- and temporal-restricted generation and turnover of phosphoinositides (PIs) by a cascade of PI-metabolizing enzymes is a key regulatory mechanism in the endocytic pathway. Here, we demonstrate that the Sac1 domain–containing protein Sac2 is a PI 4-phosphatase that specifically hydrolyzes phosphatidylinositol 4-phosphate in vitro. We further show that Sac2 colocalizes with early endosomal markers and is recruited to transferrin (Tfn)-containing vesicles during endocytic recycling. Exogenous expression of the catalytically inactive mutant Sac2C458S resulted in altered cellular distribution of Tfn receptors and delayed Tfn recycling. Furthermore, genomic ablation of Sac2 caused a similar perturbation on Tfn and integrin recycling as well as defects in cell migration. Structural characterization of Sac2 revealed a unique pleckstrin-like homology Sac2 domain conserved in all Sac2 orthologues. Collectively, our findings provide evidence for the tight regulation of PIs by Sac2 in the endocytic recycling pathway.

Introduction

Phosphoinositides (PIs) are unique and specialized lipids in that their headgroup, myo-inositol ring, can be reversibly phosphorylated at the 3′, 4′, and 5′ positions to generate seven distinct biologically active PI isoforms. Although comprising <10% of total phospholipids, PIs are essential regulators of many cellular processes such as cell signaling, cytoskeleton dynamics, and membrane trafficking (Odorizzi et al., 2000; De Matteis and Godi, 2004; Di Paolo and De Camilli, 2006). PIs have a heterogeneous distribution in different membranes, thus allowing selective recruitment of proteins containing PI recognition modules to specific organelle membranes. The maintenance of the selective distribution of specific PI species, as well as the dynamic control of PI composition in response to acute signaling inputs is achieved by a large number of PI kinases and phosphatases (Balla, 2013).

The Sac1 domain–containing proteins constitute one essential family of the PI phosphatases. In vertebrates, five genes have been identified to contain the Sac1 homology domain, which include Sac1, Sac2, Sac3/Fig4, and synaptojanin 1 and 2. The founding member of this family, Sac1, is a transmembrane protein localized to the ER and the Golgi apparatus and plays a major role in the homeostasis of phosphatidylinositol 4-phosphate (PI(4)P; Whitters et al., 1993; Nemoto et al., 2000). Sac3/Fig4 has been shown to regulate PI(3,5)P_2 levels at lysosomes or yeast vacuoles (Rudge et al., 2004; Duex et al., 2006) and genetic mutations in Sac3/Fig4 lead to several diseases, including an autosomal recessive Charcot-Tooth disorder (CMT4J) and a subset of amyotrophic lateral sclerosis in human (Chow et al., 2007, 2009). Synaptojanin 1 and 2 are unique members in that each contains a Sac1 domain, which dephosphorylates PI(3)P and PI(4)P, and a 5-phosphatase domain, which dephosphorylates PI(4,5)P_2 and PI(3,4,5)P_3 (McPherson et al., 1996; Guo et al., 1999).

Among the Sac1 domain–containing proteins, Sac2 remains the least well understood. Sac2 is a 128-kD protein encoded by the gene *INPP5F*. Besides the conserved N-terminal Sac1 domain, Sac2 contains a unique homology domain, homology Sac2 (hSac2), followed by a proline-rich C-terminal portion with various lengths in different species. Sac2 is an evolutionarily conserved protein in multicellular organisms from nematode to human. Sac2 orthologues are also found in fungi genera such as *Aspergillus* species and *Yarrowia lipolytica*, but is absent in *Saccharomyces cerevisiae*. Initial cloning and characterization of human Sac2 showed that this enzyme exhibited

Correspondence to Yuxin Mao: ym253@cornell.edu

Abbreviation used in this paper: CCP, clathrin-coated pit; CI-M6PR, cation-independent mannose 6-phosphate receptor; CRISPR, clustered regularly interspaced short palindromic repeats; hSac2, homology Sac2; N2A, Neuro-2A; OCRL, oculocerebrorenal syndrome of Lowe; PH, pleckstrin homology; PI, phosphoinositide; PI(4)P, phosphatidylinositol 4-phosphate; Tfn, Transferrin; TfnR, Transferrin receptor; WT, wild type.

The Rockefeller University Press $30.00
J. Cell Biol. Vol. 209 No. 1 97–110
www.jcb.org/cgi/doi/10.1083/jcb.201408027

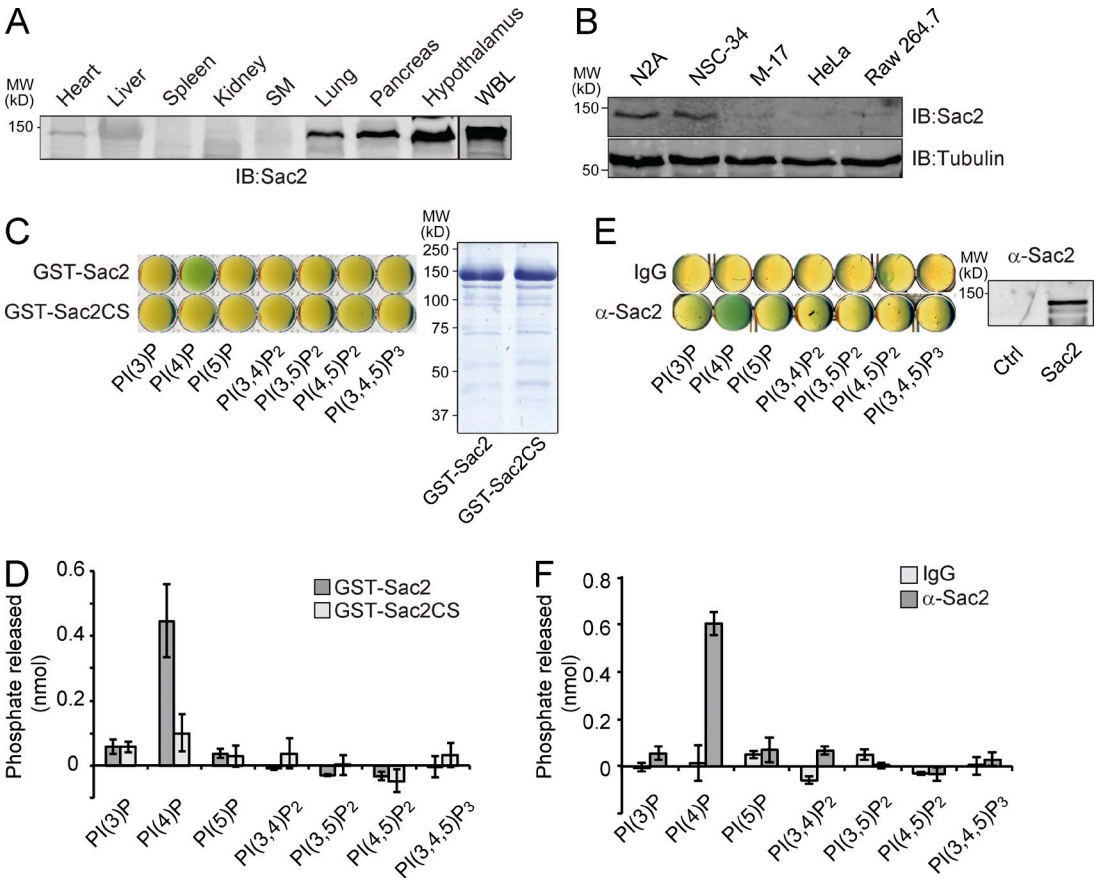

Figure 1. **Sac2 is a PI 4-phosphatase that specifically hydrolyzes PI(4)P.** (A) Mouse tissue lysates were normalized and analyzed by Western blot with specific anti-Sac2 antibody. WBL, whole mouse brain lysate. (B) Different cell lines were harvested and analyzed by Western blot with anti-Sac2 and anti-tubulin antibodies. (C, left) PI phosphatase assay with recombinant Sac2 proteins purified from insect cells. (right) SDS-PAGE analysis of the purified Sac2 samples. (D) Quantification of phosphatase assays shown in C. (E, left) Phosphatase assay with endogenous Sac2 immunopurified by anti-Sac2 antibody. (right) Western blot with anti-Sac2 of the purified protein samples. (F) Quantification of the assay shown in E. Data are from three replicate experiments (mean ± SEM).

5-phosphatase activity specific for $PI(4,5)P_2$ and $PI(3,4,5)P_3$ to generate PI(4)P and $PI(3,4)P_2$, respectively (Minagawa et al., 2001). In line with this activity, Sac2 was shown to hydrolyze $PI(3,4,5)P_3$ and thereby inactivate Akt signaling, leading to the attenuation of heart hypotrophy (Trivedi et al., 2007). Moreover, Sac2-deficient mice displayed abnormal fetal gene reactivation and increased susceptibility to stress-induced heart hypertrophy. In contrast, Sac2 transgenic mice prevented the animal from developing these symptoms (Zhu et al., 2009).

Despite these findings, many functional aspects of Sac2 are still not well understood. For example, Sac2 has a distinct enzymatic activity compared with Sac1 despite sharing a highly conserved Sac1 domain. In addition, the cellular role of Sac2 remains elusive. In this study, we demonstrate that, in contrast to a previous study (Minagawa et al., 2001), endogenous as well as purified recombinant Sac2 proteins solely hydrolyze PI(4)P. We also show that Sac2 is present at endosomal structures, which are positive for early endosomal markers Rab4 and Rab5, and partially with endocytic recycling marker Rab11, but not late endosomal markers Rab7 or Rab9. We further reveal that the exogenous expression of a catalytically inactive form of Sac2 or ablation of Sac2 by the clustered regularly interspaced short palindromic repeats (CRISPR) technique reduces transferrin (Tfn) receptor (TfnR) and β1 integrin surface levels and delays their recycling. Furthermore, Sac2 knockout cells display a severe defect in cell migration, suggesting a link between recycling and motility. In addition, we solved the crystal structure of a unique domain, hSac2, and implicated its role in Sac2 dimerization and intracellular localization. Overall, our data support a specialized role of Sac2 in the endocytic pathway through the spatiotemporal control of PI(4)P.

Results

Sac2 is highly expressed in the brain

Sac2 mRNA transcripts are found ubiquitously expressed but more enriched in the brain, heart, skeletal muscles, kidney, and placenta as revealed by Northern blot analyses (Minagawa et al., 2001). Using specific polyclonal antibodies generated against the unique hSac2 domain (aa 593–760 of human Sac2), we were able to detect the tissue distribution of Sac2 at protein levels. We found that Sac2 has the highest expression levels in the whole adult mouse brain, as well as the hypothalamus tissue (Fig. 1 A). Sac2 protein is also detected at high levels in the lung and the pancreas and at lower levels in the heart. Contrary to the Northern blot data, there is no detectable Sac2 protein in

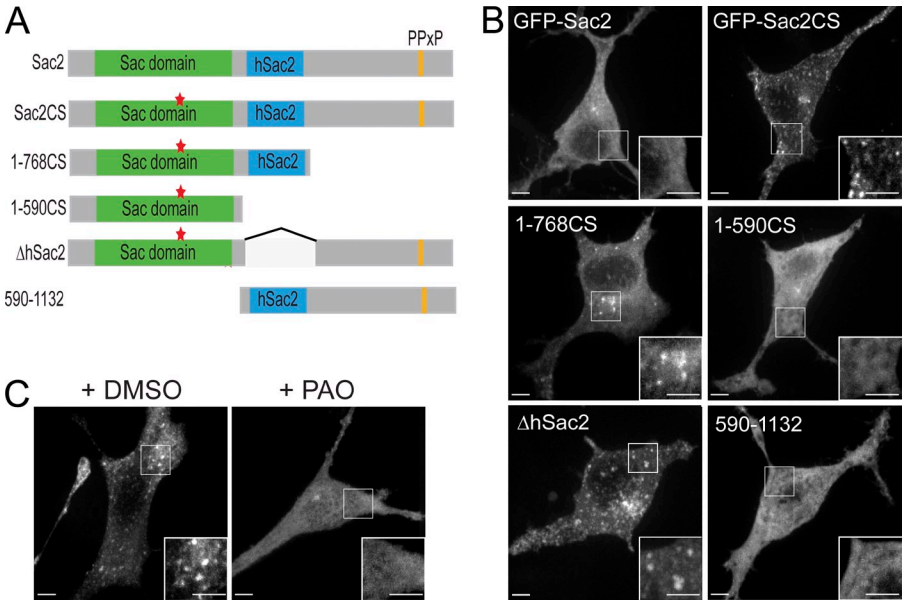

Figure 2. **Sac2CS mutant localizes to punctate structures.** (A) Schematic diagram of various constructs used in B. The C458S catalytically inactive mutation is denoted with an asterisk. (B) Confocal images of N2A cells that were transfected with GFP-Sac2, GFP-Sac2CS, or various Sac2 truncation plasmids containing an N-terminal GFP tag. (C) N2A cells were first transfected with GFP-Sac2CS for 24 h and then subjected to phenylarsine oxide (PAO; 20 µM) treatment for 10 min at 37°C. Bars, 5 µm.

the kidney and the skeletal muscle (Fig. 1 A). Consistent with the high protein levels in the brain, Sac2 is highly expressed in several neuronal cell lines, such as Neuro-2A (N2A) and NSC-34 (Fig. 1 B). These data suggest that Sac2 plays an important role in neuronal functions or in brain development. We thus chose the mouse neuroblastoma N2A cell line for subsequent experiments unless otherwise specified.

Sac2 is a PI 4-phosphatase

We next reinvestigated the enzymatic activity of Sac2. It has been reported that Sac2 is a 5-phosphatase that removes the 5′ phosphate from the inositol ring of PI(4,5)P_2 and PI(3,4,5)P_3 (Minagawa et al., 2001). However, the Sac1 domain from Sac1 or synaptojanins has been shown in in vitro phosphatase assays to predominantly dephosphorylate PI(3)P and PI(4)P and weakly against PI(3,5)P_2 (Guo et al., 1999). Given the high primary sequence homology between Sac1 and Sac2 (Manford et al., 2010; Hsu and Mao, 2014), it is surprising that Sac2 is a PI 5-phosphatase capable of hydrolyzing di- and tri- phosphorylated PI species exclusively. To resolve this apparent discrepancy, GST-tagged full-length human Sac2 protein was expressed and purified from insect cells. In contrast to a previous study (Minagawa et al., 2001), GST-Sac2 exhibited specific phosphatase activity toward PI(4)P but no activity on either PI(4,5)P_2 or PI(3,4,5)P_3. Furthermore, a single amino acid mutation of the catalytic cysteine (C458S) completely obliterated the enzymatic activity of Sac2 (Fig. 1, C and D). To test whether the observed activity of Sac2 is conserved in other species, endogenous mouse Sac2 from N2A cells was immunoprecipitated using the Sac2 polyclonal antibody. Similarly, mouse Sac2 also exhibited enzymatic activity toward PI(4)P exclusively (Fig. 1, E and F). The specific phosphatase activity is also observed with either GFP- or Flag-tagged Sac2 proteins expressed and affinity purified from HEK293T cells (Fig. S1). Collectively, these data demonstrate that Sac2 is a PI 4-phosphatase that specifically hydrolyzes PI(4)P to phosphatidylinositol.

The catalytically inactive mutant of Sac2 is localized to punctate structures

To detect the intracellular localization of Sac2, we first attempted to use our Sac2 antibodies to probe endogenous Sac2 in N2A cells. Although the antibody was able to recognize Sac2 from cell lysates by Western blots, we were unable to detect endogenous Sac2 signal by immunostaining using this antibody. To overcome this problem, N2A cells were transiently transfected with GFP-tagged Sac2 (GFP-Sac2) wild type (WT) or various Sac2 mutants (Fig. 2 A). WT Sac2 showed a cytoplasmic localization (Fig. 2 B). However, the catalytically inactive mutant GFP-Sac2CS displayed a punctate distribution in N2A cells (Fig. 2 B). Both the C-terminal truncation mutant Sac2 1-768CS and ΔhSac2 (the hSac2 domain deleted) displayed a punctate distribution. However, the catalytic domain alone (1–590) or the entire C-terminal region (590–1132) failed to localize to the punctate structures when expressed in N2A cells (Fig. 2 B). These data suggest that the puntate localization of Sac2 requires both the catalytic domain and either the hSac2 domain or its C-terminal proline-rich domain. Because the main substrate of Sac2 is PI(4)P, we next determined the dependency of Sac2-positive punctate structures on PI(4)P. When N2A cells expressing GFP-Sac2CS were treated with the phosphatidylinositol-4-kinase inhibitor phenylarsine oxide (Vieira et al., 2005), GFP-Sac2CS became diffused and cytosolic while the proteins remained punctate localized in control cells treated with DMSO (Fig. 2 C). These observations suggest that GFP-Sac2CS puncta are not caused by protein misfolding or aggregation. Instead, the GFP-Sac2CS proteins are likely recruited and trapped to its substrate PI(4)P on these punctate structures because of the loss of its catalytic activity.

Sac2 is localized to early and recycling endosomal structures

To examine the nature of Sac2CS puncta, we performed colocalization analyses with a series of membrane compartment markers. Sac2CS was detected at a small fraction of clathrin-coated pits (CCPs) as indicated by the limited partial colocalization

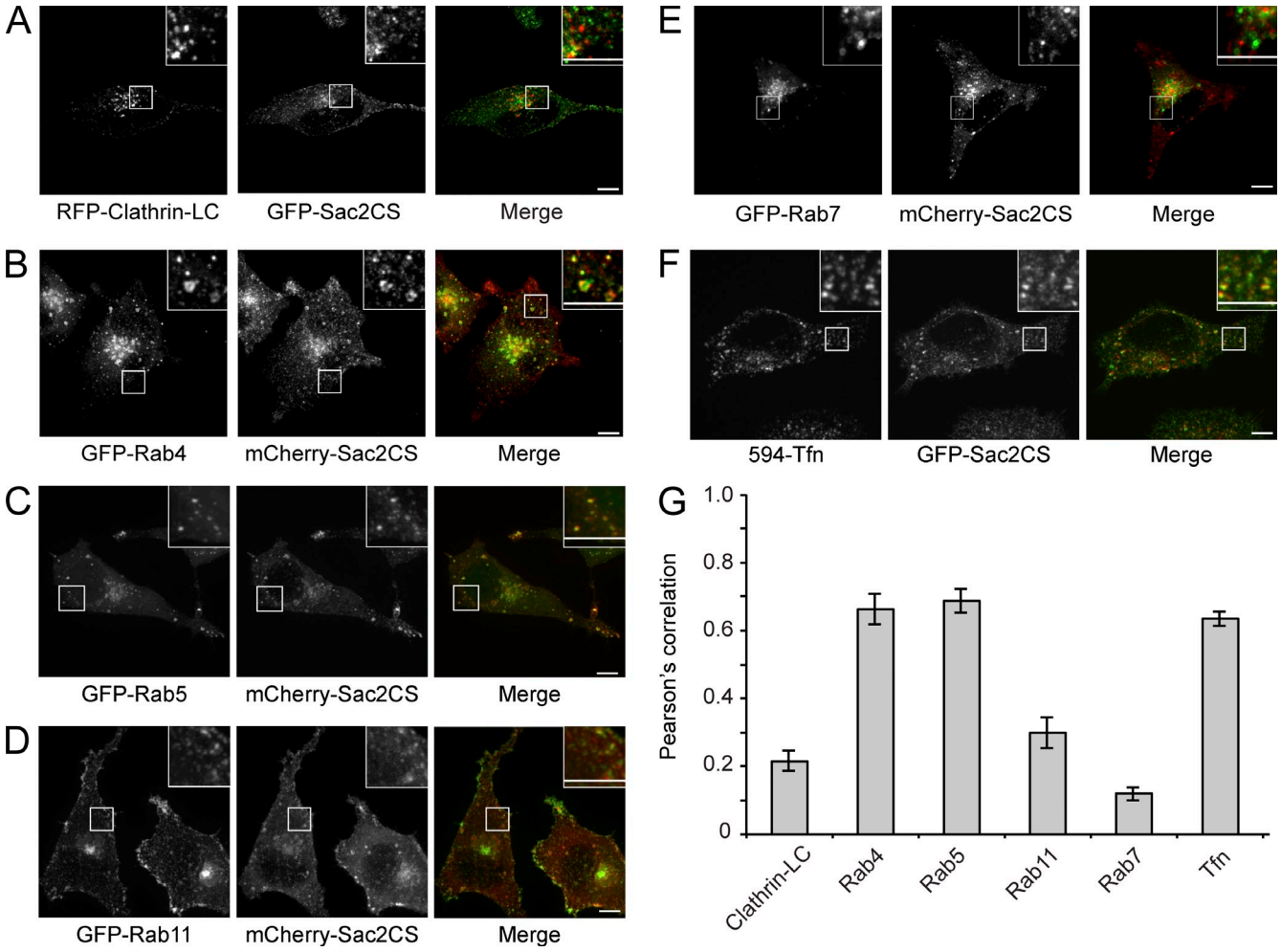

Figure 3. **Sac2 localizes to early and recycling endosomes.** (A–E) Colocalization of either GFP- or mCherry-Sac2CS with various endocytic markers. A single plane of spinning disk confocal microscopy is shown. (F) Colocalization analysis of GFP-Sac2CS with Tfn. N2A cells were transfected with GFP-Sac2CS and were treated with Alexa594-Tfn for 15 min before fixation for imaging. Bars, 5 µm. (G) Colocalization analysis of Sac2CS with various endocytic markers. The mean values of the Pearson's correlation coefficient from three cells and the SEM are shown.

with RFP-tagged clathrin light chain (Fig. 3, A and G; and Video 1). A significant colocalization of Sac2CS was observed with early endosomal marker Rab4 and Rab5 (Fig. 3, B, C, and G; and Videos 2 and 3). Sac2CS also displayed a partial colocalization with Rab11 recycling vesicles and the endocytic recycling compartment at the perinuclear region (Fig. 3, D and G; and Video 4). In contrast, little or no colocalization of Sac2CS was observed with late endosomal markers Rab7 and Rab9, and the lysosomal marker LAMP1 (Fig. 3, E and G; Fig. S2, A, B, and G; and Videos 5 and 6). To exclude the possibility that the perinuclear signal could be Golgi apparatus, we also stained cells expressing GFP-Sac2CS with antibodies against the Golgi resident protein GPP130. Very little overlap between Sac2CS and GPP130 was seen (Fig. S2 C). Furthermore, when these cells were treated with Brefeldin A, the GPP130 signal disappeared at the perinuclear region, whereas GFP-Sac2CS remained unaffected (Fig. S2 D), suggesting that GFP-Sac2CS does not localize to the Golgi apparatus. Collectively, these data are consistent with Sac2 being associated with the peripheral early endosomes and juxanuclear endocytic recycling compartment.

The cellular localization of Sac2 at early endosomal structures implies a role of Sac2 in early endocytic events. We thus examined the colocalization of Sac2 with endocytic cargoes. Cells expressing GFP-Sac2CS were either stained with monoclonal anti-TfnR antibodies or labeled with Alexa Fluor 594–Tfn and chased for 15 min. Sac2CS displayed significant colocalization with Tfn and TfnR in the punctate structures (Fig. 3, F and G; and Fig. S2, E and G). Live cell imaging also showed the active recruitment of GFP-Sac2CS proteins to Tfn-containing puncta (Video 7). To assess whether Sac2 specifically functions at the early stages of the endosomal recycling pathway rather than the late endosomal–lysosomal degradation pathway, we examined the colocalization of Sac2CS with EGF, an endocytic cargo targeted to lysosomes for degradation. HeLa cells, which express high levels of EGFR, were transfected with GFP-Sac2CS and labeled with Alexa Fluor 555–EGF followed by chase for 15 min. In contrast to Tfn, GFP-Sac2CS showed little colocalization with EGF (Fig. S2, F and G). These observations suggest that Sac2 is selectively recruited to endocytic cargoes that are programmed for recycling.

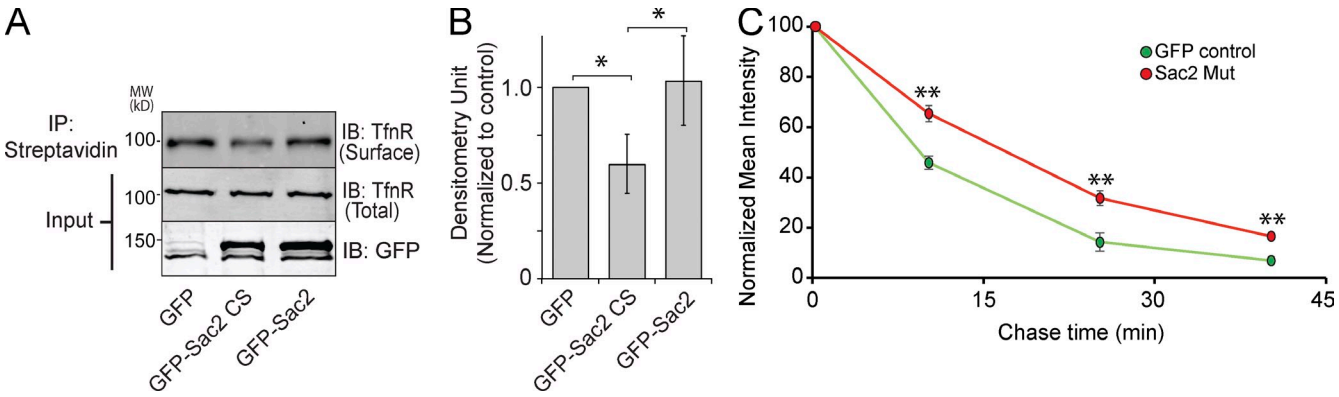

Figure 4. **Expression of Sac2CS mutant perturbs TfnR distribution and Tfn recycling.** (A) Western blot analysis of biotin surface-labeled TfnR. (B) Densitometry analysis of the Western blot images shown in A. Data are from three replicate experiments (mean ± SEM). (C) Flow cytometry analysis of Tfn recycling in N2A cells expressing GFP (control) or GFP-Sac2CS. Data are from three replicate experiments (n = 5,000 in each time point; mean ± SEM). *, $P < 0.05$; **, $P < 0.01$.

Sac2CS mutant alters the cellular distribution of TfnR and perturbs its recycling

To examine the role of Sac2 in the endocytic recycling of cell surface receptors, we first measured the steady-state ratio of TfnR levels on the cell surface versus the interior. N2A cells were transfected with GFP, GFP-Sac2CS, or GFP-Sac2 for 48 h, and then shifted to 4°C to halt endocytosis. Cell surface proteins were biotinylated with Sulfo-NHS-SS-biotin. Biotinylated surface proteins were isolated from cell lysates using streptavidin agarose beads, and the amount of surface TfnR was quantified using Western blot. A significant reduction (~30%) in the protein levels of surface TfnR was observed in cells expressing GFP-Sac2CS compared with either GFP control or WT Sac2, whereas the total levels of TfnR were similar in all three conditions (Fig. 4, A and B). These data suggest that exogenous expression of Sac2CS reduces the surface presentation of TfnR at steady state. We next examined the effect of Sac2 on the dynamics of Tfn and TfnR recycling. The kinetics of Tfn recycling was monitored by pulse-chase flow cytometry assays. Within the first 10 min, the Tfn fluorescent signal in control cells was reduced to 45.8%. However, the Tfn signal in cells expressing GFP-Sac2CS decreased only to 65.3% (Fig. 4 C). Retardation of Tfn recycling persisted to later time points (Fig. 4 C). Together, the pulse-chase data support a role of Sac2 in the regulation of Tfn recycling.

CRISPR-mediated knockout of Sac2 delays TfnR recycling

To further investigate the role of Sac2 in Tfn recycling, we generated N2A mutant cell lines with a complete disruption of Sac2 expression by the CRISPR technique (Horvath and Barrangou, 2010; Cong et al., 2013; Fig. S3). Similar to cells transiently expressing Sac2CS, Sac2 null cells showed a reduced surface distribution of TfnR (Fig. 5, A and B). In agreement with the notion that Sac2 plays a role in Tfn recycling, pulse-chase flow cytometry analyses showed a delayed recycling of Tfn in Sac2 null cells (Fig. 5 C). More importantly, this delay of Tfn recycling was restored by the reexpression of WT GFP-Sac2 in Sac2 null cells (Fig. 5 C). The effect on Tfn recycling in Sac2 null cells was visualized by confocal microscopy. Cells were labeled with Alexa Fluor 647–Tfn and chased at the indicated time points (Fig. 5 D). A prominent retention of intracellular Tfn signals was observed in Sac2 null cells at later time points, which again suggests a delay in Tfn recycling (Fig. 5 D). Notably, the reduced surface signal and delayed Tfn recycling in Sac2 null cells were rescued by expressing WT Sac2 (Fig. 5 D). Together, these data demonstrate that Sac2 is an important regulator in the Tfn/TfnR recycling pathway.

CRISPR-mediated knockout of Sac2 perturbs integrin distribution and recycling

To assess whether Sac2 has a general impact on the recycling of other endocytic cargos, we analyzed integrin recycling in Sac2 null cells. We first compared the surface distribution of β1 integrin in WT and ΔSac2 cells by flow cytometry. Surface labeling revealed that the cell surface β1 integrin levels were reduced by ~20% in Sac2 null cells, whereas the total β1 integrin levels were similar (Fig. 6, A–C). Immunostaining with anti–β1 integrin under nonpermeabilized and permeabilized conditions further showed that the β1 integrin signal was significantly weaker at the cell surface in ΔSac2 cells compared with WT cells (Fig. 6 D, top). In contrast to the cell surface levels of β1 integrin, a stronger intracellular β1 integrin signal was detected in ΔSac2 cells after permeabilization, whereas the total β1 integrin levels were similar (Fig. 6 D, bottom). These results suggest that, similar to TfnR, the intracellular distribution of β1 integrin, but not the total protein levels, was also perturbed when Sac2 was deleted. We then examined the effect of Sac2 on integrin recycling by an antibody-labeling pulse-chase experiment. In WT cells, internalized antibody–receptor complexes efficiently recycled back to the cell surface within 20 min, whereas in Sac2 null cells, significantly lower amounts were returned (Fig. 6 E, top). On the contrary, more labeled integrins were retained intracellularly in ΔSac2 cells compared with WT cells (Fig. 6 E, bottom), suggesting that integrin recycling is delayed in Sac2 null cells.

To assess whether Sac2 specifically affects endocytic recycling processes rather than other membrane trafficking events

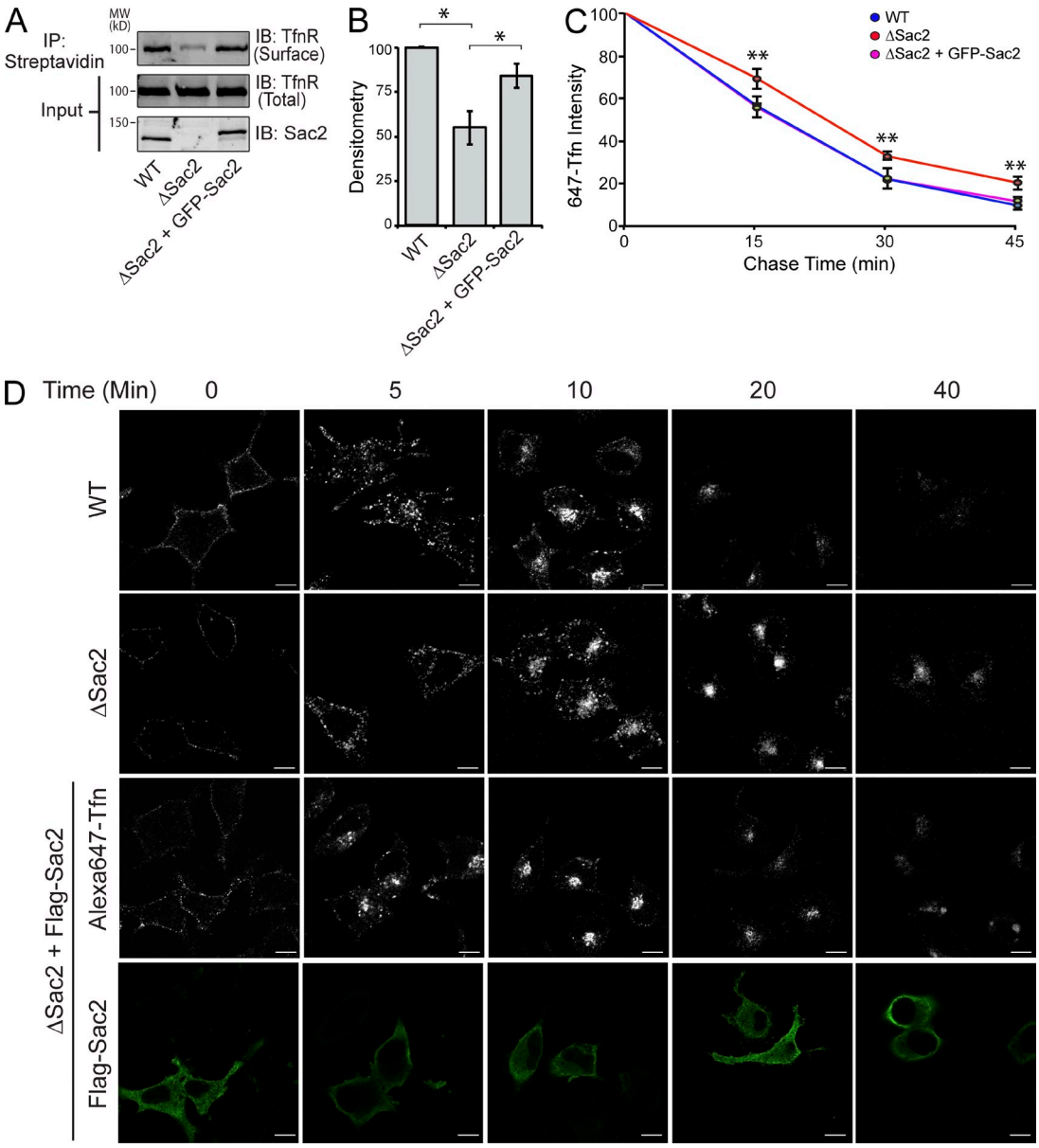

Figure 5. **Defects of Tfn recycling in Sac2 null cells.** (A) Western blot analysis of biotin surface-labeled TfnR. (B) Quantification was performed as in Fig. 4 B. Values are normalized to WT cells (surface/total). Data are from three replicate experiments (mean ± SEM). (C) Flow cytometry analysis of Tfn recycling in WT and Sac2 null N2A cells. Data are from three replicate experiments (n = 5,000 in each time point; mean ± SEM). (D) Representative images of Tfn recycling at the indicated times points. (bottom) Cells transfected with Flag-Sac2 (green). Bars, 10 µm. *, P < 0.05; **, P < 0.01.

such as retrograde trafficking, we examined the localization of a chimeric form of the cation-independent mannose 6-phosphate receptor (CI-M6PR), which at steady state resides mostly in the perinuclear TGN region, but in conditions where retrograde trafficking is impaired, the receptor switches from a perinuclear region to peripheral structures or gets degraded (Seaman, 2004, 2007). WT and Sac2 null cells were cotransfected with GFP-CI-M6PR and DsRed-GalT, a TGN marker. We did not observe any changes in colocalization with DsRed-GalT or fluorescence signal of CI-M6PR between WT and Sac2 null cells (Fig. S4). Collectively, these data suggest that Sac2 is specifically involved in the endocytic recycling of several cell surface receptors but not in other membrane trafficking pathways such as retrograde trafficking.

Tfn-containing compartment is positive for PI(4)P in Sac2 null cells

Our data showed that Sac2 specifically hydrolyzes PI(4)P and regulates Tfn recycling. These data led us to hypothesize that in Sac2 null cells, PI(4)P may transiently accumulate at the compartments where Tfn is enriched. To detect this pool of PI(4)P, we used two commonly used pleckstrin homology (PH) domains from FAPP1 and OSBP (Levine and Munro, 2002; Godi et al., 2004; He et al., 2011) and the PI(4)P-binding domain of SidC (P4C; Dolinsky et al., 2014) as specific in vivo PI(4)P probes. WT and Sac2 null cells were transfected with GFP-2xPH^{FAPP1} for overnight and then labeled with Alexa Fluor 647–Tfn. Live imaging was performed to monitor the in vivo PI(4)P dynamics. In WT cells, the PI(4)P probe predominantly labeled the

Golgi apparatus with very little colocalization with Tfn (Fig. 7, A and B). However, in Sac2 null cells, the PI(4)P probe not only strongly labeled the Golgi area, but also labeled punctate structures scattered in the cytoplasm and some of these labeled puncta were also positive for Tfn, suggesting that PI(4)P indeed transiently accumulates on Tfn-containing endosomal structures in Sac2 null cells. The increased levels of PI(4)P on Tfn-positive endosomal structures were completely reversed when WT mCherry-Sac2 was reintroduced into Sac2 null cells (Fig. 7, A and B). Similar results were observed when OSBP (Fig. 7, C and D) or P4C probes were used (not depicted). These observations suggest that Sac2 deletion causes a transient accumulation of PI(4)P on Tfn-positive endosomal structures and the hydrolysis of PI(4)P by Sac2 is critical for the endocytic recycling of cell surface receptors.

Sac2 null cells are defective in cell migration

Endocytic recycling of cell surface cargo receptors is essential for cell motility and migration (Jones et al., 2006; Fletcher and Rappoport, 2010). Studies have shown that perturbations on endocytic functions that result in reduced plasma membrane proteins, such as integrin and TfnR, lead to defects in cell migration (Rappoport and Simon, 2003; White et al., 2007; Majeed et al., 2014). To test whether Sac2 play a role in cell migration, we performed wound-healing assays. In response to monolayer wounding, the migration velocity of Sac2 null cells was significantly slower (~1.1 µm/h) compared with WT cells (2.6 µm/h; Fig. 8, A and B). The defect in cell migration in Sac2 null cells was rescued to a rate of ~1.8 µm/h by exogenous expression of GFP-Sac2 (Fig. 8, A and B). Together, our data support a role of Sac2 in cell migration.

Structure of the hSac2

Sac2 has a unique conserved hSac2 domain and our data suggest that the hSac2 domain contributes to its intracellular localization (Fig. 2). To understand the molecular basis, we performed structural studies of this unique domain (aa 593–760). The hSac2 domain contains ~120 aa of unknown function and structure. Sequence homology searches reveal homology sequence in proteins encoded by the transformation-related protein 63 regulated 1 (TPRG1; Antonini et al., 2008) and the tumor protein p63-regulated gene 1-like genes (TPRGL; Kremer et al., 2007). The hSac2 domain was expressed, purified, and crystallized. The hSac2 crystal diffracted to 2.7 Å and the structure was solved by single wavelength anomalous dispersion method (Table S1). The hSac2 domain consists of a core of two perpendicularly apposed β sheets with a C-terminal α helix that seals the gap between two β sheets (Fig. 9 A). This core has a similar architecture to the PH domain (Fig. S5 A). In addition to the core, hSac2 has an extra N-terminal α helix and a short β strand at the C-terminal end. PH domains are known to bind to PIs. However, hSac2 did not show any binding to any phospholipids in our liposome sedimentation assays (unpublished data). Electrostatic surface potential calculation did not reveal any surface patch with significant positive electrostatic potentials (Fig. S5, B and C), which are frequently observed in many lipid-binding

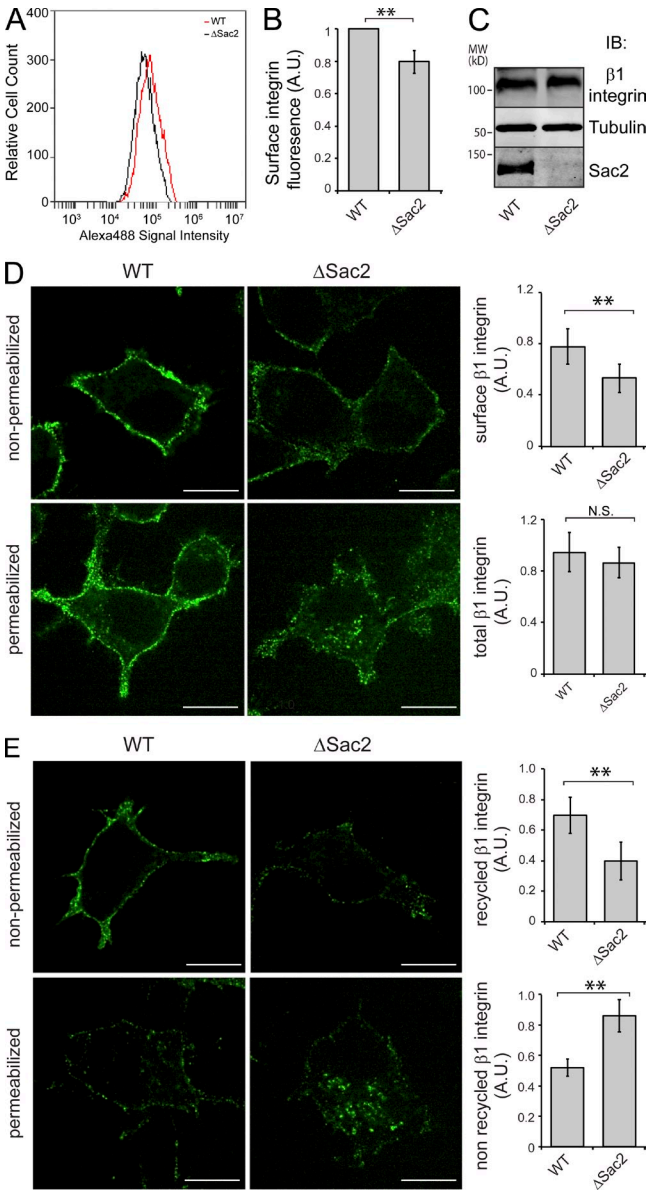

Figure 6. **Defects of integrin recycling in Sac2 null cells.** (A) Flow cytometry analysis of surface integrin in WT (black) and ΔSac2 (red) cells. (B) Quantitative analysis of the mean intensity shown in A. Data are from three replicate experiments (n = 10,000; mean ± SEM). (C) Western blot probed with anti–β1 integrin, anti-tubulin, and anti-Sac2 of cell lysates prepared from WT and Sac2 null cells. (D) Intracellular distribution of β1 integrin in WT and ΔSac2 cells. The mean fluorescence intensity in nonpermeabilized and permeabilized cells and the SEM are shown in the right panels (n = 5). (E) Recycling assay of β1 integrin. Bars, 10 µm. The mean recycled fluorescence intensity in nonpermeabilized and permeabilized cells and the SEM are shown in the right panels (n = 5). **, P < 0.01.

modules. Our structure further revealed that the hSac2 domain may form a dimer (Fig. 9 B). The dimer interface mainly consists of the β1 strand and α2 helix in each monomer and embeds several hydrophobic residues. The dimer is further stabilized by four pairs of main chain hydrogen bonds formed between the two β1 strands within each monomer. Furthermore, dimerization of hSac2 creates a continuous anti-parallel β sheet with a large hydrophobic surface, which is covered by the N-terminal α1 helix in a swapped manner (Fig. 9 B). To test whether

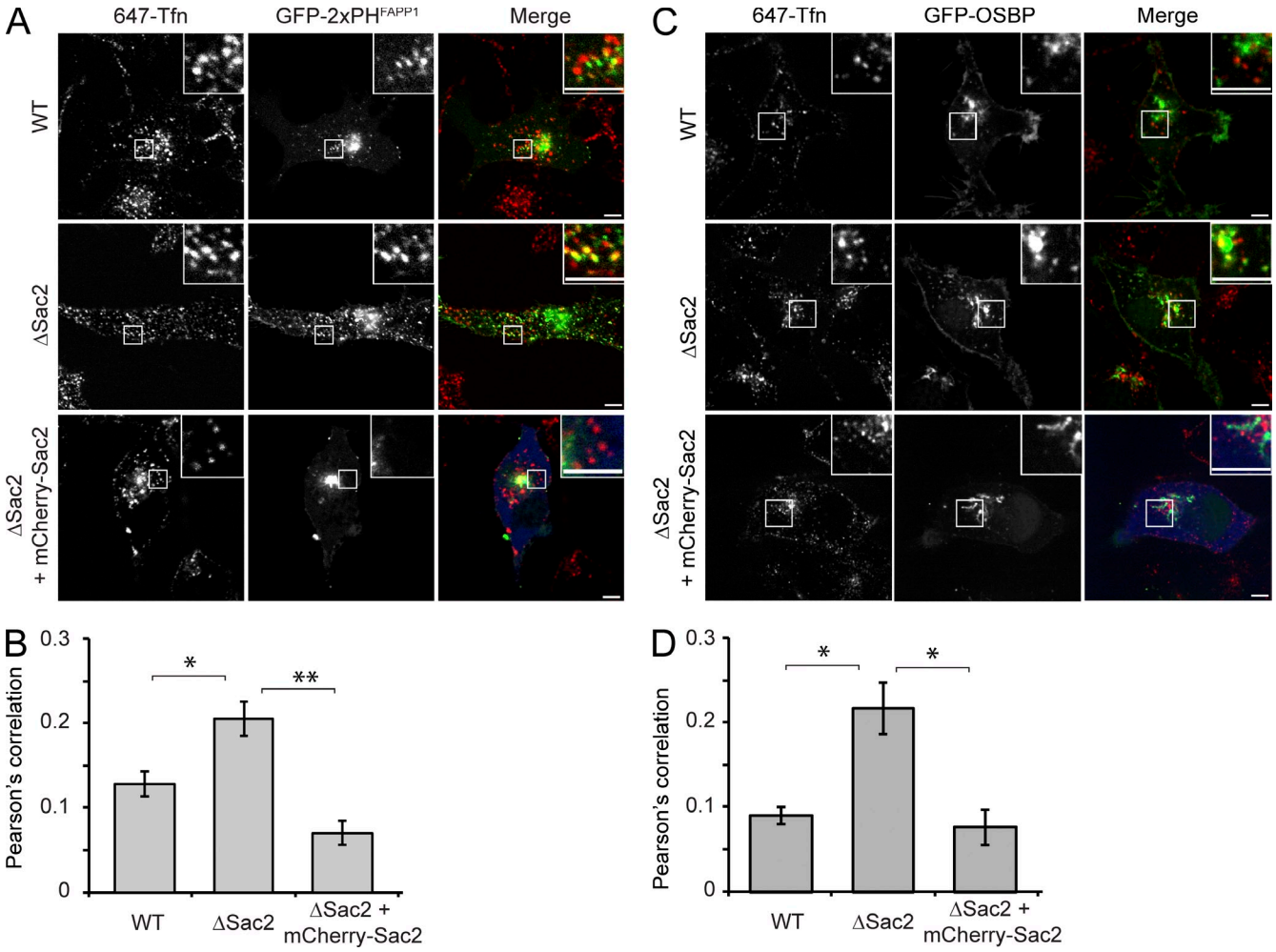

Figure 7. **Tfn-containing vesicles are positive for PI(4)P in Sac2 null cells.** (A) Colocalization assay of GFP-2xPH^{FAPP1} (green) with Alexa647-Tfn. (B) Pearson's correlation analysis of the colocalization in A. (C) Colocalization assay of GFP-PH^{OSBP} (green) with Alexa647-Tfn. (D) Pearson's correlation analysis of the colocalization in C. Error bars represent SEM. mCherry-Sac2 was pseudo-colored in blue. Bars, 5 µm. *, $P < 0.05$; **, $P < 0.01$.

Sac2 indeed forms a dimer and whether the hSac2 domain contributes to the Sac2 dimerization, a coimmunoprecipitation experiment was performed using constructs containing the catalytic and hSac2 domains (aa 1–798). Flag- and GFP-tagged Sac2 1–798 were cotransfected in HEK293T cells and cell lysates were immunoprecipitated with anti-Flag beads. Coimmunoprecipitated proteins were analyzed by Western blot probing for both Flag and GFP tags. Flag-Sac2 1–798 coprecipitated a significant amount of GFP-Sac2 1–798 (Fig. 9 C). However, the interaction was significantly reduced with GFP-Sac2 1–567 (lacking the hSac2 domain). Collectively, our structural data suggest that the hSac2 domain is at least partially responsible for the Sac2 dimerization and may contribute to the endosomal localization of Sac2 through potential protein–protein interactions but not by direct lipid binding.

Discussion

The hSac2 domain is a unique signature for Sac2

Based on sequence homology, the hSac2 domain family has been annotated by the Pfam database as a conserved domain family found in eukaryotes. In all Sac2 orthologues, the hSac2 domain is associated with the Sac1 phosphatase domain and serves as a unique signature that distinguishes Sac2 from other Sac1 domain–containing phosphatases. Thus, it is likely that the hSac2 domain may have unique functions, such as membrane targeting and/or protein–protein interactions for the recruitment of Sac2 to the endocytic recycling pathway. Interestingly, Sac2 is absent in *S. cerevisiae*, which seems to be in agreement with the fact that yeast does not recycle cargoes from endosomes directly back to the plasma membrane (Pelham, 2002). We determined the first crystal structure of the hSac2 domain from human Sac2. The structure reveals that hSac2 domain has a PH domain–like fold. Similar to other PH-like domains found in two homologous PI 5-phosphatases, oculocerebrorenal syndrome of Lowe (OCRL) and INPP5B (Mao et al., 2009), the hSac2 domain lacks a cationic pocket; thus, it does not bind to phospholipids. However, our data showed that hSac2 may form a dimer and is responsible for the intracellular localization of Sac2, presumably via yet unknown protein–protein interactions.

Sac2 plays a role in the endocytic pathway

It is well established that $PI(4,5)P_2$ is enriched in and serves as a marker for the plasma membrane (De Matteis and Godi,

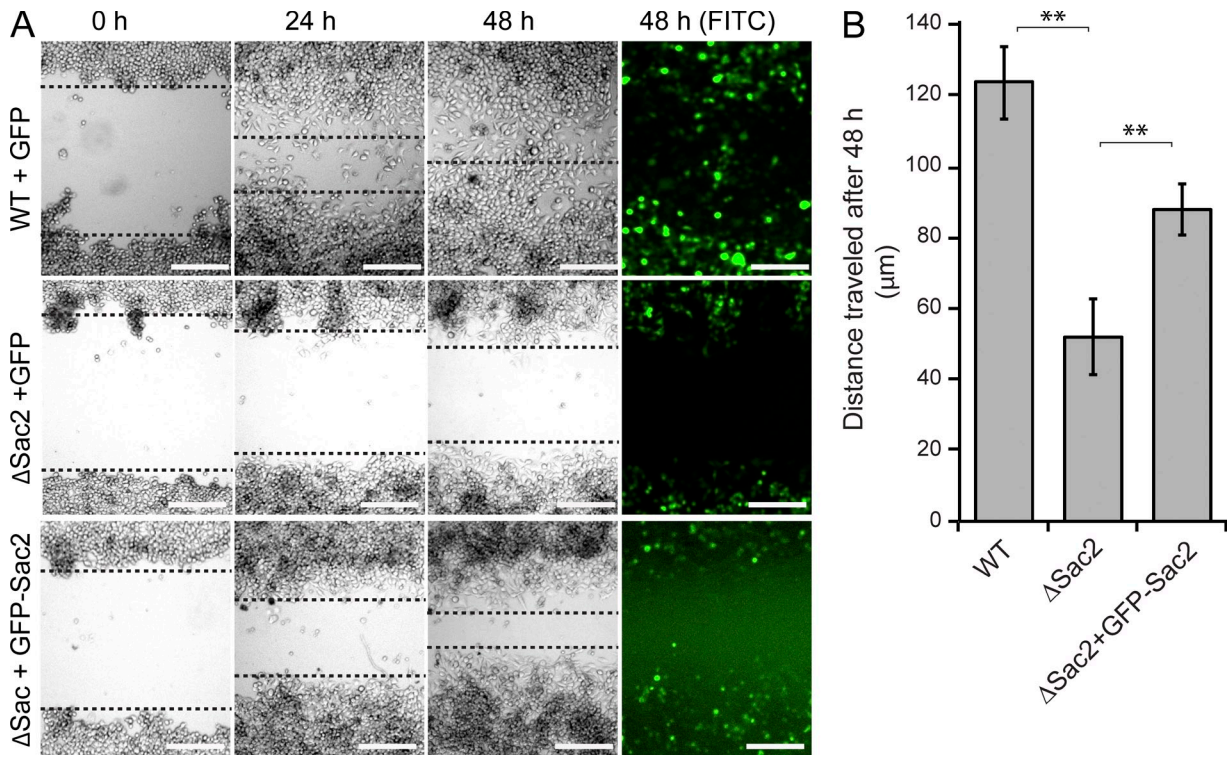

Figure 8. **Sac2 deletion delays cell migration.** (A) Wound healing assay of ΔSac2 cells. Dashed lines measure the distance of the wound. FITC images are shown to indicate transfected cells. Bars, 20 μm. (B) Quantification of the distance traveled after 48 h as measured by the dashed lines. Data are from three replicate experiments (mean ± SEM; **, $P < 0.01$).

2004). $PI(4,5)P_2$ functions as a coreceptor at the plasma membrane to recruit several endocytic proteins including subunits of AP-2, AP180/CALM, epsin, and dynamin to trigger the formation of CCPs (McMahon and Boucrot, 2011). These $PI(4,5)P_2$ molecules are quickly degraded during the subsequent endocytic stages. Several PI phosphatases contribute to the removal of $PI(4,5)P_2$. For example, the PI phosphatase synaptojanin is recruited to CCPs and dephosphorylates $PI(4,5)P_2$ to facilitate the uncoating of CCPs (Cremona et al., 1999) and the release of $PI(4,5)P_2$-binding adaptor proteins. The PI 5-phosphatase SHIP-2 (SH2 domain–containing inositol 5-phosphatase) is localized to endocytic CCPs and controls the maturation of CCPs (Nakatsu et al., 2010). OCRL, another inositol 5-phosphatase that acts on both $PI(4,5)P_2$ and $PI(3,4,5)P_3$, is associated with newly formed clathrin-coated vesicles (Erdmann et al., 2007; Mao et al., 2009). By converting $PI(4,5)P_2$ into PI(4)P during the endocytic pathway, PI 5-phosphatases may contribute to the establishment of a new PI identity of early endosomes to regulate downstream receptor trafficking and sorting. However, the enzymatic cascade following the actions of 5-phosphatases that eventually leads to the conversion of $PI(4,5)P_2$ to PI(3)P at early endosomes is still not well understood. One plausible pathway is through the interplay of PI kinases and phosphatases. Recent data show that the class II PI 3-kinase C2α controls clathrin-mediated endocytosis by the phosphorylation of PI(4)P to $PI(3,4)P_2$ (Posor et al., 2013). It also has been shown that the PI 4-phosphatase, INPP4A, which specifically hydrolyzes $PI(3,4)P_2$ to PI(3)P (Norris et al., 1995), contributes to the production of PI(3)P on early endosomes (Shin et al., 2005).

In contrast with the previously reported activity, which indicates that Sac2 is a PI 5-phosphatase capable of hydrolyzing di- and tri-phosphorylated lipids (Minagawa et al., 2001), we observed that recombinant GST-hSac2 has a specific enzymatic activity toward PI(4)P. We speculate the discrepancy might be a result of the impurity of the enzymes used in Minagawa et al. (2001). In this work, the specific activity of Sac2 against PI(4)P was further supported by enzymatic activity observed from recombinant human Sac2 or endogenous Sac2 purified from mammalian cells (Fig. 1, E and F; and Fig. S1). Thus, we conclude that Sac2 is a 4-phosphatase that specifically hydrolyzes PI(4)P. We provide evidence that Sac2 associates with early endocytic compartments, particularly with the endocytic recycling cargo Tfn and its receptor TfnR. Our data identify Sac2, a previously poorly characterized PI phosphatase, as a novel player in the endocytic pathway. These results uncover an alternative mechanism on the conversion of $PI(4,5)P_2$ during endocytosis and allow us to propose a working model (Fig. 10). In this model, 5-phosphatases, such as OCRL, may function upstream to hydrolyze $PI(4,5)P_2$ to PI(4)P. Sac2 is recruited to clathrin-coated vesicles and early endosomes to relay the dephosphorylation reaction by hydrolyzing PI(4)P to phosphatidylinositol, which can be directly phosphorylated by hVps34 to generate PI(3)P (Simonsen et al., 1998). Thus, through an enzymatic cascade of 5-phosphatases, Sac2, and PI 3-kinases, the initial $PI(4,5)P_2$ that is required for clathrin-dependent endocytosis

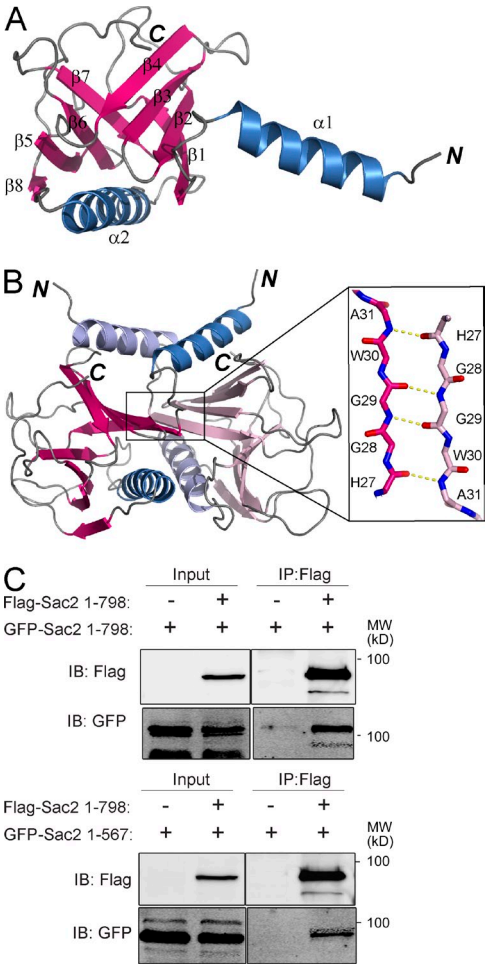

Figure 9. **Crystal structure of the hSac2 domain of Sac2.** (A) Ribbon diagram of the overall structure of the hSac2 domain. The hSac2 domain consists of a core of two perpendicularly apposed β sheets (pink) with a C-terminal α helix (blue). (B) Ribbon diagram of the hSac2 dimer. (inset) A zoom-in view showing the four pairs of main chain hydrogen bond formed between the two β1 strands within each monomer. (C) Western blot showing Flag-Sac2 1–798 coimmunoprecipiting with GFP-Sac2 1–798 but much reduced with GFP-Sac2 1–567.

is converted to PI(3)P, which is a key lipid for subsequent endosomal functions. As predicted by this model, ablation of Sac2 function by CRISPR-mediated genome editing causes transient accumulation of PI(4)P on the early endosomes and delays the recycling of Tfn and integrin.

We also showed that the catalytically inactive mutant of Sac2CS, but not the WT Sac2, is localized to punctate structures in the cell, which are positive for endocytic markers and recycling cargos. We speculate that the formation of Sac2CS-positive puncta is likely a result of the following scenarios. First, Sac2CS is fully functional to engage in binding with PI(4)P without hydrolysis, thus prolonging the enzyme–substrate interaction and forming a more stable complex. Second, the dominant-negative effect of Sac2CS may induce the accumulation of PI(4)P on endosomes, which may enhance the binding of Sac2CS to PI(4)P. The third reason could be that an unknown Sac2 recruiting factor has a higher affinity for endosome association because of the accumulation of PI(4)P on endosomes. Because the C-terminal portion of Sac2 is required

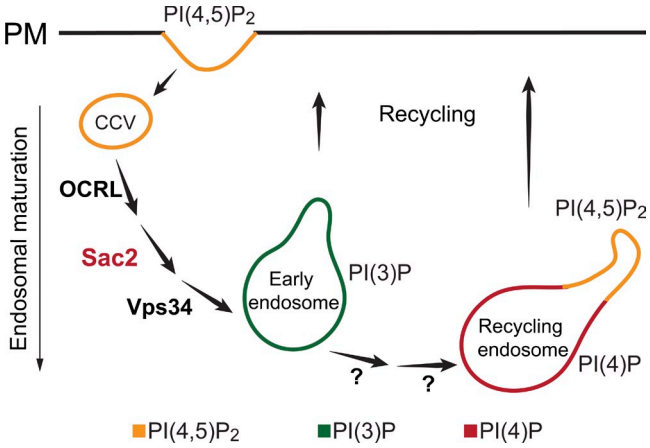

Figure 10. **Model for Sac2 function during endosomal recycling.** The recycling process is dependent on the proper control of PIs. Initial stage of endocytosis requires the hydrolysis of $PI(4,5)P_2$ to PI(4)P via PI 5-phosphatases, such as OCRL. Sac2 is then recruited to endocytic intermediates to hydrolyze PI(4)P to phosphatidylinositol, which is a substrate for Vps34 to generate PI(3)P. The spatiotemporal conversion from $PI(4,5)P_2$- to PI(3)P-enriched endosome is essential for endosomal maturation and subsequent recycling events.

for the formation of Sac2CS puncta, it is likely that the hSac2 domain and/or proline-rich domain play a role in the recruitment of Sac2 to the endosomal intermediate structures via the association with this unknown factor that is specifically localized on endosomes, but not on the Golgi complex.

The role of Sac2 in the regulation of cardiac hypotrophy

Sac2 was reported to attenuate cardiac hypertrophy via inactivation of the PI 3-kinase–dependent signaling pathway (Trivedi et al., 2007). It was proposed that the decrease in PI 3-kinase–Akt signaling is caused by the down-regulation of $PI(3,4,5)P_3$ by the 5-phosphatase activity of Sac2. However, we demonstrate here that Sac2 is a PI 4-phosphatase that specifically hydrolyzes PI(4)P and plays a role in endocytic membrane trafficking. Effects of membrane trafficking on signaling have been well documented. Membrane trafficking regulates the balance between degradation and recycling of signaling receptors and hence, modulates the signal quality, duration, and magnitude (Lemmon and Schlessinger, 2010; Platta and Stenmark, 2011). Cellular signaling processes are also governed by the assembly and turnover of signal transduction complexes, which in turn are regulated by PIs on the endosomal surface (Zoncu et al., 2009). Thus, we propose that the inhibition of PI 3-kinase–Akt signaling may be caused by the altered endocytic trafficking of signaling receptors, such as receptor tyrosine kinases or G protein–coupled receptors. However, the exact molecular connection between the cellular function of Sac2 to cardiac hypotrophy remains to be elucidated.

The role of Sac2 in neurological functions

Our data showed that Sac2 is highly expressed in the brain tissue and neuronal cells (Fig. 1, A and B). We further showed that Sac2 regulates the endocytic recycling pathway and plays a role in cell migration. Accumulating evidence suggests that

endosomal trafficking is essential in neurite outgrowth and has a pathogenic role in several neurological disorders (Sann et al., 2009; Li and DiFiglia, 2012). For example, Rab11-positive endosomes were shown to supply membrane materials for neurite outgrowth (Albertinazzi et al., 2003). In primary cortical neurons derived from mice modeled for Huntington's disease, the activity of Rab11 and hence the recycling of cargoes, such as TfnR, was impaired (Li et al., 2010). In contrast, neuronal cell migration is also shown to be a fundamental mechanism for brain development and neural circuitry establishment (Marín et al., 2010; Cooper, 2013). Thus, it is likely that Sac2 plays a role in neuronal development and functions. Although Sac2 knockout and transgenic mice have been created (Zhu et al., 2009), and these mice showed cardiac hypotrophy–related phenotypes, no defects in the nervous system were reported. However, given the high Sac2 protein levels in brain tissues and the function of Sac2 in endosomal recycling and cell migration in cultured N2A cells, we would expect to see some neurological defects in the nervous system in Sac2 knockout mice. Future works on neuronal development and function in these mouse models are required to answer this question.

In conclusion, our data demonstrate that Sac2 is a PI 4-phosphatase that specifically hydrolyzes PI(4)P. We further provide evidence that Sac2 participates in endocytic recycling processes by facilitating the lipid conversion of $PI(4,5)P_2$ along the vesicle trafficking route from CCPs to early endosomes (Fig. 10). Our data underscore the importance of spatial and temporal control of PIs along the endocytic pathway by a cascade of PI-metabolizing enzymes. Our results will pave the way for further studies on the role of Sac2 in neuronal physiology and development.

Materials and methods

Cloning, mutagenesis, and plasmids

PCR products for full-length Sac2 (aa 1–1133) and different Sac2 truncations amplified from cDNA encoding human Sac2 were digested with BamHI and NotI restriction enzymes and inserted into pEGFP-C1 with CMV promoter (Takara Bio Inc.) or pCmCherry (the GFP in the vector pEGFP-C1 was replaced with mCherry via EcoRI site) in frame with the N-terminal GFP or mCherry tag, respectively. Flag-tagged Sac2 was generated using BglII and SalI restriction sites in the plasmid p3xFlag-CMV7.1. Single amino acid substitution (C458S) of Sac2 was introduced by site-directed mutagenesis. For bacteria expression, hSac2 (aa 593–760) was cloned into a pET28a-based vector with T7 promoter in frame with an N-terminal His-SUMO tag. The expression plasmids for rabs, M6PR, and GalT were obtained from B. Brown and A. Bretcher (Cornell University, Ithaca, NY). The rab4 (aa 1–218), rab5 (aa 1–215), rab7 (aa 1–207), rab9 (aa 1–201), and rab11 (aa 1–216) were inserted using BamHI and NotI sites into pEGFP-C1 (Kuroda et al., 2002). The CI-M6PR was cloned into the pEGFP-C1 vector backbone encoding a chimeric protein composed of an N-terminal signal peptide from preproglucagon cDNA including 21 residues from the N terminus of the glucagon synthetic precursor followed by EGFP, a linker of six residues, and the transmembrane and cytoplasmic domains of CI-MPR that were generated from mouse CI-M6PR cDNA. (Waguri et al., 2003). The Golgi GalT (aa 1–379) was cloned into pDsRed-monomer (Takara Bio Inc.) in frame with the N-terminal DsRed tag. The gene encoding human clathrin light chain (aa 1–248) was inserted using NheI and BglII in frame with the N-terminal TagRFP (Evrogen) into the C1 cloning vectors (Takara Bio Inc.; Shaner et al., 2008). The PI(4)P probe P4C was cloned from *Legionella pneumophila* SidC (aa 614–744) and inserted into pEGFP-C1.

Cell culture, transfection, and Western blot

N2A and HeLa cells were grown in DMEM supplemented with 10% FBS (Cellgro) and 1% Pen/Strep (Cellgro) at 37°C in 5% CO_2 atmosphere. All plasmids were transfected using polyethyleneimine (PEI) reagent. Mouse tissue lysates (gift from L. Qi, Cornell University, Ithaca, NY) and cell lysates were resuspended in 2× SDS loading buffer containing 100 mM Tris-HCl, pH 7.0, 4% SDS, 0.2% bromophenol blue, 20% glycerol, and 200 mM DTT. Samples were analyzed by Western blot probed with anti-rabbit Sac2 antibody used at 1:1,000.

CRISPR

Guide sequence in the first exon of Sac2 (5′-GCTGCAGGCCGCCGTCGCGC-3′) was designed and chosen using Feng Zhang laboratory's target finder (Fig. S3). The insert was cloned into pX330 (Addgene) via the BbsI site. The pX330 vector with human U6 promoter containing the Sac2 guide insert was transfected with PEI reagent. After transfection for 24 h, N2A cells were counted and diluted in complete medium to a density of 100 cells. The cells were grown 5–7 d until the appearance of colony formation. Individual colony was trypsinized and reseeded to 24-well plate. A total of 30 clones were screened for endogenous Sac2 protein level by Western blot with anti-rabbit Sac2 antibody (Covance). Two Sac2 null clones were isolated.

Immunofluorescence

Cells were seeded on glass coverslips and fixed in 4% PFA/PBS for 15 min. Cells were washed twice with PBS and permeabilized in PBS containing 0.05% saponin and 3% BSA for 30 min. Cells were immunostained with proper primary and secondary antibodies. Anti–mouse Lamp1 (BD), anti–mouse TfnR (Invitrogen), and anti–rabbit GPP130 (Covance) antibodies were used at 1:1,000, 1:500, and 1:500, respectively. Disruption of Golgi apparatus was performed with 5 µg/ml of Brefeldin A (Sigma-Aldrich) for 15 min at 37°C. Confocal images, acquired at room temperature, were taken using a CSU-X spinning disk microscope (Intelligent Imaging Innovations) with a spherical aberration correction device, 63×, 1.4 NA objective, on an inverted microscope (Leica), and acquired with a QuantEM EMCCD camera using Slidebook software (Intelligent Imaging Innovations). Image resizing, cropping, and brightness were uniformly adjusted in Photoshop (Adobe).

Quantitative analysis of colocalization and total cell fluorescence

Fiji program was used to process images. To quantify the degree of colocalization between Sac2CS and different organelle markers, three cells were selected, and for each cell, the entire cell region was examined. Pearson's correlation coefficient was calculated using Fiji plug-in Coloc2 program on a single plane between the two indicated fluorescent signals (Adler and Parmryd, 2010). ImageJ was used to measure cell fluorescence. P-value was calculated using Student's *t* test).

Time-lapse microscopy

For live cell imaging, cells were plated in a 35-mm Petri dish, 14-mm glass bottom microwell. Cells were transfected as described in the Cell culture, transfection, and Western blot section. Before imaging, medium was replaced with Hepes-buffered DMEM without phenol red (Lonza). All time-lapse movies were captured with a confocal microscope (LSM 700; Carl Zeiss) using a 63× oil immersion objective (Carl Zeiss) at 37°C. Single section images were recorded at 5- to 10-s intervals and processed using the Zen software (Carl Zeiss). For imaging Tfn recycling, cells were first starved for 2 h in DMEM-free medium and, before image capture, were replaced with complete medium containing 5 µg/ml of Alexa Fluor 647–Tfn at 37°C.

Tfn and integrin recycling assay

For immunostaining, cells were grown on glass coverslips and starved for 30 min in DMEM-free medium at 37°C and then labeled with 10 µg/ml of Alexa Fluor 594–Tfn for 30 min in HBSS, 20 mM Hepes, and 2 mg/ml BSA on ice for 30 min. After wash with cold PBS, cells were chased for different time points in complete medium containing 50-fold excessive of unlabeled Tfn and 100 µM deferoxamine to prevent reinternalization. At the end of each time point, cells were washed with 0.1 M glycine, pH 3.5, for 1 min and followed by a wash with PBS. Cells were then fixed in 4% PFA. The coverslips were washed twice in PBS and then mounted on a microscope slide with Fluoromount-G for imaging.

For the antibody-induced recycling assay, cells were incubated with 5 µg/ml of rat anti–β1 integrin (gift from D. Holowka, Cornell University, Ithaca, NY; FCMAB269F; EMD Millipore) in complete medium for 1 h at 37°C. The cells were first washed with PBS and treated with 0.1 M glycine, pH 2.5, twice for 1 min to remove surface-bound antibody. After additional wash with PBS, cells were returned to 37°C in complete medium to

chase internalized antibody back to the cell surface. For the analysis of surface receptor level, cells were washed in PBS, fixed in 4% PFA for 20 min, blocked in 1% BSA in PBS for 15 min, and incubated with anti-rat Alexa Fluor 488. For the analysis of internal receptor level, cells were treated with 0.1 M glycine, pH 2.5, twice for 1 min to remove recycled surface antibody–receptor complex. Cells were fixed in 4% PFA, permeabilized in 0.1% saponin for 30 min, and incubated with the secondary antibody anti–rat Alexa Fluor 488.

Flow cytometry

N2A cells were detached using trypsin and serum starved in suspension for 30 min at 37°C in DMEM. For labeling, cells were incubated with 10 µg/ml of Alexa Fluor 647–Tfn in buffer solution containing HBSS, 20 mM Hepes, and 2 mg/ml BSA at 4°C for 30 min. Unbound Tfns were removed by washing the cells twice with PBS. Cells were then supplemented in complete medium with 50 µg/ml of unlabeled Tfn and 100 µM deferoxamine and transferred to 37°C. After 5 min of incubation, cells were sampled at time 0, 10, 20, and 40 min. At each time point, Cells were washed in 0.1 M glycine, pH 3.5, followed by fixation in 2% PFA for 15 min. Fixed cells were resuspended in PBS before subjecting to flow cytometry analysis. 5,000 cells were analyzed by measuring Alexa Fluor 647 fluorescence. Time points are normalized time 0 and plotted for cell-associated Alexa Fluor 647 signal intensity.

For detection of surface β1 integrin, cells were detached with 10 mM EDTA in PBS for 20 min at 37°C, followed by washing with PBS. The resuspended cells were incubated in 50 µl of diluted anti–β1 integrin (1:15; FCMAB269F; EMD Millipore) in PBS containing 2% FBS for 30 min on ice. Cells were washed one time in PBS and then incubated with anti–rat Alexa Fluor 488 (1:100) in PBS containing 10% FBS for 30 min on ice. Cells were washed again with PBS and fixed in 2% PFA for 15 min. 10,000 cells were analyzed on an Accuri flow cytometer.

Biotin surface labeling

N2A cells were starved in DMEM-free medium for 2 h at 37°C in 5% CO_2 incubator. Cells were then washed twice with HBSS buffer before labeling with 1 mg/ml of Sulfo-NHS-SS-Biotin (ProteoChem) in HBSS for 30 min on ice. Cells were washed twice with HBSS to remove excess biotin and subsequently harvested in HBSS containing 1% Triton X-100 and protease inhibitor. After centrifugation, an aliquot was collected as input for total protein levels, and the lysate was incubated with streptavidin resin (GenScript) at 4°C for 2 h. The resin was then washed three times in lysis buffer followed by addition of SDS loading buffer. Western blot was performed and probed with mouse anti-TfnR and rabbit anti-Sac2 antibodies.

Scratch wound healing assay

WT N2A cells and ΔSac2 cells were transfected with the corresponding plasmid. The next day, transfected cells were seeded in triplicate in a 96-well plate in a density that after 24 h, 90% confluence is reached as a monolayer. Wound was applied by scratching the monolayer with a 10-µl pipette tip across the center of the well. Each well was washed one time with PBS to remove the detached cells and replaced with fresh medium. Images were captured at 0, 24, and 48 h with a microscope (ImageXpress-MICRO; Molecular Devices) using a 4× objective transmitted light lens and FITC filter set to identify transfected cells. The experiment was performed twice in triplicate (n = 6).

Immunoprecipitation

HEK293T cells grown to ∼80% confluence were cotransfected with appropriate plasmids using PEI reagent. After ∼18-h transfection, cells were lysed in RIPA buffer. Soluble fractions were collected by centrifugation at 18,000 rpm for 15 min at 4°C. Immunoprecipitates were prepared by 2-h binding at 4°C, followed by washing with 50 mM Tris-HCl, pH 8.0, and 150 mM NaCl. To prepare Sac2 proteins for enzymatic assays, endogenous mouse Sac2 proteins from N2A cells were immunopurified using 1 µg of anti-Sac2 antibodies and 15 µl of protein A beads. GFP-Sac2 and Flag-Sac2 proteins were purified using GFP-Trap beads (ChromoTek) and anti-Flag M2 affinity gel (Sigma-Aldrich), respectively. Final beads were resuspended in reaction buffer (50 mM Tris-HCl, pH 8.0, and 150 mM NaCl). Endogenous β1 integrin was detected using rabbit anti–β1 integrin (Cell Signaling Technology).

Enzymatic assays

All diC8-PIs were purchased from Cell Signaling Technology. All reactions were performed in a polystyrene 96-well plate for 20 min at 37°C with a total volume of 50 µl of reaction mixture, which contains reaction buffer, 1 nmol of lipids, and 2 µl of bead slurry of immunoprecipitated purified proteins. The reaction was quenched by the addition of malachite green solution containing 0.1% Tween. The amount of phosphate release was measured at OD 620 absorbance and was compared with inorganic phosphate standards.

Protein expression and purification

The hSac2 domain was expressed as His-SUMO fusion in *Escherichia coli* and was purified by Co^{2+} resins. The His-SUMO–tagged protein was cleaved by sumo protease Ulp1 and the protein was further purified by gel filtration. The protein was concentrated to 10 mg/ml in 20 mM Tris, pH 7.8, and 20 mM NaCl for crystallization. For Sac2 full-length protein expression, *Tni* insect cells were seeded in a 500-ml culture flask containing 200 ml of culture media. Recombinant proteins were purified with GSH sepharose resins.

Crystallization

Crystals were grown at room temperature by the hanging-drop vapor diffusion method by mixing 1 µl of protein (11 mg/ml) with an equal volume of reservoir solution containing 0.2 M ammonium sulfate, 0.1 M Tris-HCl, pH 8.0, and 20% PEG3350. Rod-shaped crystals were formed within 2–3 d.

Data collection, processing, structure determination, and refinement

Diffraction datasets for selenomethionine protein crystals were collected at the Cornell High Energy Synchrotron Source. All datasets were indexed, integrated, and scaled with HKL-2000 (Otwinowski and Minor, 1997). Selenomethionines were identified in the crystal using the program HKL2MAP (Pape and Schneider, 2004). Iterative cycles of model building and refinement were performed with the program COOT (Emsley and Cowtan, 2004) and the refmac5 program (Murshudov et al., 1997) in the CCP4 suite (Collaborative Computational Project, Number 4, 1994) to complete the final model.

Atomic coordinates and structure factors for the reported structures have been deposited into the Protein Data Bank under accession no. 4XUU.

Online supplemental material

Fig. S1 shows PI phosphatase assay with GFP- and Flag- tagged Sac2. Fig. S2 shows the colocalization of Sac2CS with different endosomal and organelle markers. Fig. S3 shows the generation of Sac2 knockout cells by CRISPR technique. Fig. S4 shows the cellular distribution of CI-M6PR is unaffected in Sac2 null cells. Fig. S5 shows the structural comparison of hSac2 domain with a canonical PH domain. Table S1 shows the crystallographic statistics. Videos 1–7 show the colocalization dynamics of Sac2CS with a series of endocytic markers. Online supplemental material is available at http://www.jcb.org/cgi/content/full/jcb.201408027/DC1. Additional data are available in the JCB DataViewer at http://dx.doi.org/10.1083/jcb.201408027.dv.

We thank Dr. Anthony Bretscher for the assistance in confocal microscope, Dr. Ling Qi for mouse tissue samples, and Dr. David Holowka for integrin antibodies. We are also grateful to the staff at the Cornell High Energy Synchrotron Source (CHESS).

CHESS is supported by the National Science Foundation and National Institutes of Health (NIH)/National Institute of General Medical Sciences via National Science Foundation award DMR-0225180. The MacCHESS resource is supported by NIH/National Center for Research Resources award RR-01646. This work was supported by the Harry Samuel Mann Award (F. Hsu) and NIH grant R01-GM094347 (Y. Mao). The content is solely the responsibility of the authors and does not necessarily represent the official views of the NIH.

The authors declare no competing financial interests.

Submitted: 7 August 2014
Accepted: 5 March 2015

References

Adler, J., and I. Parmryd. 2010. Quantifying colocalization by correlation: the Pearson correlation coefficient is superior to the Mander's overlap coefficient. *Cytometry A*. 77:733–742. http://dx.doi.org/10.1002/cyto.a.20896

Albertinazzi, C., L. Za, S. Paris, and I. de Curtis. 2003. ADP-ribosylation factor 6 and a functional PIX/p95-APP1 complex are required for Rac1B-mediated neurite outgrowth. *Mol. Biol. Cell*. 14:1295–1307. http://dx.doi.org/10.1091/mbc.E02-07-0406

Antonini, D., M. Dentice, P. Mahtani, L. De Rosa, G. Della Gatta, A. Mandinova, D. Salvatore, E. Stupka, and C. Missero. 2008. Tprg, a gene predominantly

expressed in skin, is a direct target of the transcription factor p63. *J. Invest. Dermatol.* 128:1676–1685. http://dx.doi.org/10.1038/jid.2008.12

Balla, T. 2013. Phosphoinositides: tiny lipids with giant impact on cell regulation. *Physiol. Rev.* 93:1019–1137. http://dx.doi.org/10.1152/physrev.00028.2012

Chow, C.Y., Y. Zhang, J.J. Dowling, N. Jin, M. Adamska, K. Shiga, K. Szigeti, M.E. Shy, J. Li, X. Zhang, et al. 2007. Mutation of FIG4 causes neurodegeneration in the pale tremor mouse and patients with CMT4J. *Nature*. 448:68–72. http://dx.doi.org/10.1038/nature05876

Chow, C.Y., J.E. Landers, S.K. Bergren, P.C. Sapp, A.E. Grant, J.M. Jones, L. Everett, G.M. Lenk, D.M. McKenna-Yasek, L.S. Weisman, et al. 2009. Deleterious variants of FIG4, a phosphoinositide phosphatase, in patients with ALS. *Am. J. Hum. Genet.* 84:85–88. http://dx.doi.org/10.1016/j.ajhg.2008.12.010

Collaborative Computational Project, Number 4. 1994. The CCP4 suite: programs for protein crystallography. *Acta Crystallogr. D Biol. Crystallogr.* 50:760–763. http://dx.doi.org/10.1107/S0907444994003112

Cong, L., F.A. Ran, D. Cox, S. Lin, R. Barretto, N. Habib, P.D. Hsu, X. Wu, W. Jiang, L.A. Marraffini, and F. Zhang. 2013. Multiplex genome engineering using CRISPR/Cas systems. *Science*. 339:819–823. http://dx.doi.org/10.1126/science.1231143

Cooper, J.A. 2013. Cell biology in neuroscience: mechanisms of cell migration in the nervous system. *J. Cell Biol.* 202:725–734. http://dx.doi.org/10.1083/jcb.201305021

Cremona, O., G. Di Paolo, M.R. Wenk, A. Lüthi, W.T. Kim, K. Takei, L. Daniell, Y. Nemoto, S.B. Shears, R.A. Flavell, et al. 1999. Essential role of phosphoinositide metabolism in synaptic vesicle recycling. *Cell*. 99:179–188. http://dx.doi.org/10.1016/S0092-8674(00)81649-9

De Matteis, M.A., and A. Godi. 2004. PI-loting membrane traffic. *Nat. Cell Biol.* 6:487–492. http://dx.doi.org/10.1038/ncb0604-487

Di Paolo, G., and P. De Camilli. 2006. Phosphoinositides in cell regulation and membrane dynamics. *Nature*. 443:651–657. http://dx.doi.org/10.1038/nature05185

Dolinsky, S., I. Haneburger, A. Cichy, M. Hannemann, A. Itzen, and H. Hilbi. 2014. The *Legionella longbeachae* Icm/Dot substrate SidC selectively binds phosphatidylinositol 4-phosphate with nanomolar affinity and promotes pathogen vacuole-endoplasmic reticulum interactions. *Infect. Immun.* 82:4021–4033. http://dx.doi.org/10.1128/IAI.01685-14

Duex, J.E., F. Tang, and L.S. Weisman. 2006. The Vac14p–Fig4p complex acts independently of Vac7p and couples $PI3,5P_2$ synthesis and turnover. *J. Cell Biol.* 172:693–704. http://dx.doi.org/10.1083/jcb.200512105

Emsley, P., and K. Cowtan. 2004. Coot: model-building tools for molecular graphics. *Acta Crystallogr. D Biol. Crystallogr.* 60:2126–2132. http://dx.doi.org/10.1107/S0907444904019158

Erdmann, K.S., Y. Mao, H.J. McCrea, R. Zoncu, S. Lee, S. Paradise, J. Modregger, D. Biemesderfer, D. Toomre, and P. De Camilli. 2007. A role of the Lowe syndrome protein OCRL in early steps of the endocytic pathway. *Dev. Cell.* 13:377–390. http://dx.doi.org/10.1016/j.devcel.2007.08.004

Fletcher, S.J., and J.Z. Rappoport. 2010. Moving forward: polarised trafficking in cell migration. *Trends Cell Biol.* 20:71–78. http://dx.doi.org/10.1016/j.tcb.2009.11.006

Godi, A., A. Di Campli, A. Konstantakopoulos, G. Di Tullio, D.R. Alessi, G.S. Kular, T. Daniele, P. Marra, J.M. Lucocq, and M.A. De Matteis. 2004. FAPPs control Golgi-to-cell-surface membrane traffic by binding to ARF and PtdIns(4)P. *Nat. Cell Biol.* 6:393–404. http://dx.doi.org/10.1038/ncb1119

Guo, S., L.E. Stolz, S.M. Lemrow, and J.D. York. 1999. SAC1-like domains of yeast SAC1, INP52, and INP53 and of human synaptojanin encode polyphosphoinositide phosphatases. *J. Biol. Chem.* 274:12990–12995. http://dx.doi.org/10.1074/jbc.274.19.12990

He, J., J.L. Scott, A. Heroux, S. Roy, M. Lenoir, M. Overduin, R.V. Stahelin, and T.G. Kutateladze. 2011. Molecular basis of phosphatidylinositol 4-phosphate and ARF1 GTPase recognition by the FAPP1 pleckstrin homology (PH) domain. *J. Biol. Chem.* 286:18650–18657. http://dx.doi.org/10.1074/jbc.M111.233015

Horvath, P., and R. Barrangou. 2010. CRISPR/Cas, the immune system of bacteria and archaea. *Science*. 327:167–170. http://dx.doi.org/10.1126/science.1179555

Hsu, F., and Y. Mao. 2014. The structure of phosphoinositide phosphatases: Insights into substrate specificity and catalysis. *Biochim. Biophys. Acta*. http://dx.doi.org/10.1016/j.bbalip.2014.09.015

Jones, M.C., P.T. Caswell, and J.C. Norman. 2006. Endocytic recycling pathways: emerging regulators of cell migration. *Curr. Opin. Cell Biol.* 18:549–557. http://dx.doi.org/10.1016/j.ceb.2006.08.003

Kremer, T., C. Kempf, N. Wittenmayer, R. Nawrotzki, T. Kuner, J. Kirsch, and T. Dresbach. 2007. Mover is a novel vertebrate-specific presynaptic protein with differential distribution at subsets of CNS synapses. *FEBS Lett.* 581:4727–4733. http://dx.doi.org/10.1016/j.febslet.2007.08.070

Kuroda, T.S., M. Fukuda, H. Ariga, and K. Mikoshiba. 2002. Synaptotagmin-like protein 5: a novel Rab27A effector with C-terminal tandem C2 domains. *Biochem. Biophys. Res. Commun.* 293:899–906. http://dx.doi.org/10.1016/S0006-291X(02)00320-0

Lemmon, M.A., and J. Schlessinger. 2010. Cell signaling by receptor tyrosine kinases. *Cell*. 141:1117–1134. http://dx.doi.org/10.1016/j.cell.2010.06.011

Levine, T.P., and S. Munro. 2002. Targeting of Golgi-specific pleckstrin homology domains involves both PtdIns 4-kinase-dependent and -independent components. *Curr. Biol.* 12:695–704. http://dx.doi.org/10.1016/S0960-9822(02)00779-0

Li, X., and M. DiFiglia. 2012. The recycling endosome and its role in neurological disorders. *Prog. Neurobiol.* 97:127–141. http://dx.doi.org/10.1016/j.pneurobio.2011.10.002

Li, X., A. Valencia, E. Sapp, N. Masso, J. Alexander, P. Reeves, K.B. Kegel, N. Aronin, and M. Difiglia. 2010. Aberrant Rab11-dependent trafficking of the neuronal glutamate transporter EAAC1 causes oxidative stress and cell death in Huntington's disease. *J. Neurosci.* 30:4552–4561. http://dx.doi.org/10.1523/JNEUROSCI.5865-09.2010

Majeed, S.R., L. Vasudevan, C.Y. Chen, Y. Luo, J.A. Torres, T.M. Evans, A. Sharkey, A.B. Foraker, N.M. Wong, C. Esk, et al. 2014. Clathrin light chains are required for the gyrating-clathrin recycling pathway and thereby promote cell migration. *Nat. Commun.* 5:3891. http://dx.doi.org/10.1038/ncomms4891

Manford, A., T. Xia, A.K. Saxena, C. Stefan, F. Hu, S.D. Emr, and Y. Mao. 2010. Crystal structure of the yeast Sac1: implications for its phosphoinositide phosphatase function. *EMBO J.* 29:1489–1498. http://dx.doi.org/10.1038/emboj.2010.57

Mao, Y., D.M. Balkin, R. Zoncu, K.S. Erdmann, L. Tomasini, F. Hu, M.M. Jin, M.E. Hodsdon, and P. De Camilli. 2009. A PH domain within OCRL bridges clathrin-mediated membrane trafficking to phosphoinositide metabolism. *EMBO J.* 28:1831–1842. http://dx.doi.org/10.1038/emboj.2009.155

Marín, O., M. Valiente, X. Ge, and L.H. Tsai. 2010. Guiding neuronal cell migrations. *Cold Spring Harb. Perspect. Biol.* 2:a001834. http://dx.doi.org/10.1101/cshperspect.a001834

McMahon, H.T., and E. Boucrot. 2011. Molecular mechanism and physiological functions of clathrin-mediated endocytosis. *Nat. Rev. Mol. Cell Biol.* 12:517–533. http://dx.doi.org/10.1038/nrm3151

McPherson, P.S., E.P. Garcia, V.I. Slepnev, C. David, X. Zhang, D. Grabs, W.S. Sossin, R. Bauerfeind, Y. Nemoto, and P. De Camilli. 1996. A presynaptic inositol-5-phosphatase. *Nature*. 379:353–357. http://dx.doi.org/10.1038/379353a0

Minagawa, T., T. Ijuin, Y. Mochizuki, and T. Takenawa. 2001. Identification and characterization of a sac domain-containing phosphoinositide 5-phosphatase. *J. Biol. Chem.* 276:22011–22015. http://dx.doi.org/10.1074/jbc.M101579200

Murshudov, G.N., A.A. Vagin, and E.J. Dodson. 1997. Refinement of macromolecular structures by the maximum-likelihood method. *Acta Crystallogr. D Biol. Crystallogr.* 53:240–255. http://dx.doi.org/10.1107/S0907444996012255

Nakatsu, F., R.M. Perera, L. Lucast, R. Zoncu, J. Domin, F.B. Gertler, D. Toomre, and P. De Camilli. 2010. The inositol 5-phosphatase SHIP2 regulates endocytic clathrin-coated pit dynamics. *J. Cell Biol.* 190:307–315. http://dx.doi.org/10.1083/jcb.201005018

Nemoto, Y., B.G. Kearns, M.R. Wenk, H. Chen, K. Mori, J.G. Alb Jr., P. De Camilli, and V.A. Bankaitis. 2000. Functional characterization of a mammalian Sac1 and mutants exhibiting substrate-specific defects in phosphoinositide phosphatase activity. *J. Biol. Chem.* 275:34293–34305. http://dx.doi.org/10.1074/jbc.M003923200

Norris, F.A., V. Auethavekiat, and P.W. Majerus. 1995. The isolation and characterization of cDNA encoding human and rat brain inositol polyphosphate 4-phosphatase. *J. Biol. Chem.* 270:16128–16133. http://dx.doi.org/10.1074/jbc.270.27.16128

Odorizzi, G., M. Babst, and S.D. Emr. 2000. Phosphoinositide signaling and the regulation of membrane trafficking in yeast. *Trends Biochem. Sci.* 25:229–235. http://dx.doi.org/10.1016/S0968-0004(00)01543-7

Otwinowski, Z., and W. Minor. 1997. Processing of X-ray diffraction data collected in oscillation mode. *Methods Enzymol.* 276:307–326. http://dx.doi.org/10.1016/S0076-6879(97)76066-X

Pape, T., and T.R. Schneider. 2004. HKL2MAP: a graphical user interface for macromolecular phasing with SHELX programs. *J. Appl. Crystallogr.* 37:843–844. http://dx.doi.org/10.1107/S0021889804018047

Pelham, H.R. 2002. Insights from yeast endosomes. *Curr. Opin. Cell Biol.* 14:454–462. http://dx.doi.org/10.1016/S0955-0674(02)00352-6

Platta, H.W., and H. Stenmark. 2011. Endocytosis and signaling. *Curr. Opin. Cell Biol.* 23:393–403. http://dx.doi.org/10.1016/j.ceb.2011.03.008

Posor, Y., M. Eichhorn-Gruenig, D. Puchkov, J. Schöneberg, A. Ullrich, A. Lampe, R. Müller, S. Zarbakhsh, F. Gulluni, E. Hirsch, et al. 2013.

Spatiotemporal control of endocytosis by phosphatidylinositol-3,4-bisphosphate. *Nature*. 499:233–237. http://dx.doi.org/10.1038/nature12360

Rappoport, J.Z., and S.M. Simon. 2003. Real-time analysis of clathrin-mediated endocytosis during cell migration. *J. Cell Sci.* 116:847–855. http://dx.doi.org/10.1242/jcs.00289

Rudge, S.A., D.M. Anderson, and S.D. Emr. 2004. Vacuole size control: regulation of PtdIns(3,5)P_2 levels by the vacuole-associated Vac14-Fig4 complex, a PtdIns(3,5)P_2-specific phosphatase. *Mol. Biol. Cell*. 15:24–36. http://dx.doi.org/10.1091/mbc.E03-05-0297

Sann, S., Z. Wang, H. Brown, and Y. Jin. 2009. Roles of endosomal trafficking in neurite outgrowth and guidance. *Trends Cell Biol.* 19:317–324. http://dx.doi.org/10.1016/j.tcb.2009.05.001

Seaman, M.N. 2004. Cargo-selective endosomal sorting for retrieval to the Golgi requires retromer. *J. Cell Biol.* 165:111–122. http://dx.doi.org/10.1083/jcb.200312034

Seaman, M.N. 2007. Identification of a novel conserved sorting motif required for retromer-mediated endosome-to-TGN retrieval. *J. Cell Sci.* 120:2378–2389. http://dx.doi.org/10.1242/jcs.009654

Shaner, N.C., M.Z. Lin, M.R. McKeown, P.A. Steinbach, K.L. Hazelwood, M.W. Davidson, and R.Y. Tsien. 2008. Improving the photostability of bright monomeric orange and red fluorescent proteins. *Nat. Methods*. 5:545–551. http://dx.doi.org/10.1038/nmeth.1209

Shin, H.W., M. Hayashi, S. Christoforidis, S. Lacas-Gervais, S. Hoepfner, M.R. Wenk, J. Modregger, S. Uttenweiler-Joseph, M. Wilm, A. Nystuen, et al. 2005. An enzymatic cascade of Rab5 effectors regulates phosphoinositide turnover in the endocytic pathway. *J. Cell Biol.* 170:607–618. http://dx.doi.org/10.1083/jcb.200505128

Simonsen, A., R. Lippé, S. Christoforidis, J.M. Gaullier, A. Brech, J. Callaghan, B.H. Toh, C. Murphy, M. Zerial, and H. Stenmark. 1998. EEA1 links PI(3)K function to Rab5 regulation of endosome fusion. *Nature*. 394:494–498. http://dx.doi.org/10.1038/28879

Trivedi, C.M., Y. Luo, Z. Yin, M. Zhang, W. Zhu, T. Wang, T. Floss, M. Goettlicher, P.R. Noppinger, W. Wurst, et al. 2007. Hdac2 regulates the cardiac hypertrophic response by modulating Gsk3β activity. *Nat. Med.* 13:324–331. http://dx.doi.org/10.1038/nm1552

Vieira, O.V., P. Verkade, A. Manninen, and K. Simons. 2005. FAPP2 is involved in the transport of apical cargo in polarized MDCK cells. *J. Cell Biol.* 170:521–526. http://dx.doi.org/10.1083/jcb.200503078

Waguri, S., F. Dewitte, R. Le Borgne, Y. Rouillé, Y. Uchiyama, J.F. Dubremetz, and B. Hoflack. 2003. Visualization of TGN to endosome trafficking through fluorescently labeled MPR and AP-1 in living cells. *Mol. Biol. Cell*. 14:142–155. http://dx.doi.org/10.1091/mbc.E02-06-0338

White, D.P., P.T. Caswell, and J.C. Norman. 2007. αvβ3 and α5β1 integrin recycling pathways dictate downstream Rho kinase signaling to regulate persistent cell migration. *J. Cell Biol.* 177:515–525. http://dx.doi.org/10.1083/jcb.200609004

Whitters, E.A., A.E. Cleves, T.P. McGee, H.B. Skinner, and V.A. Bankaitis. 1993. SAC1p is an integral membrane protein that influences the cellular requirement for phospholipid transfer protein function and inositol in yeast. *J. Cell Biol.* 122:79–94. http://dx.doi.org/10.1083/jcb.122.1.79

Zhu, W., C.M. Trivedi, D. Zhou, L. Yuan, M.M. Lu, and J.A. Epstein. 2009. Inpp5f is a polyphosphoinositide phosphatase that regulates cardiac hypertrophic responsiveness. *Circ. Res.* 105:1240–1247. http://dx.doi.org/10.1161/CIRCRESAHA.109.208785

Zoncu, R., R.M. Perera, D.M. Balkin, M. Pirruccello, D. Toomre, and P. De Camilli. 2009. A phosphoinositide switch controls the maturation and signaling properties of APPL endosomes. *Cell*. 136:1110–1121. http://dx.doi.org/10.1016/j.cell.2009.01.032